



Volatile fluxes through the Big Bend section of the San Andreas Fault, California: Helium and carbon-dioxide systematics

Justin T. Kulongoski ^{a,*}, David R. Hilton ^b, Peter H. Barry ^b, Bradley K. Esser ^c, Darren Hillegonds ^c, Kenneth Belitz ^a

^a U.S. Geological Survey, California Water Science Center, San Diego, CA 92101, USA

^b Scripps Institution of Oceanography, UCSD, La Jolla, CA 92024-0244, USA

^c Lawrence Livermore National Laboratory, Livermore, CA 92550, USA

ARTICLE INFO

Article history:

Accepted 5 September 2012

Available online 11 September 2012

Keywords:

San Andreas Fault System (SAFS)

Helium isotope

Groundwater

Big Bend section

Mantle volatile

Carbon dioxide flux

ABSTRACT

To investigate the source of volatiles and their relationship to the San Andreas Fault System (SAFS), 18 groundwater samples were collected from wells near the Big Bend section of the SAFS in southern California and analyzed for helium and carbon abundance and isotopes. Concentrations of ⁴He, corrected for air-bubble entrainment, vary from 4.15 to 62.7 ($\times 10^{-8}$) cm³ STP g⁻¹ H₂O. ³He/⁴He ratios vary from 0.09 to 3.52 *R_A* (where *R_A* = air ³He/⁴He), consistent with up to 44% mantle helium in samples. A subset of 10 samples was analyzed for the major volatile phase (CO₂) – the hypothesized carrier phase of the helium in the mantle–crust system: CO₂/³He ratios vary from 0.614 to 142 ($\times 10^{11}$), and $\delta^{13}\text{C}$ (CO₂) values vary from –21.5 to –11.9‰ (vs. PDB).

³He/⁴He ratios and CO₂ concentrations are highest in the wells located in the Mil Potrero and Cuddy valleys adjacent to the SAFS. The elevated ³He/⁴He ratios are interpreted to be a consequence of a mantle volatile flux though the SAFS diluted by radiogenic He produced in the crust. Samples with the highest ³He/⁴He ratios also had the lowest CO₂/³He ratios. The combined helium isotope, He–CO₂ elemental relationships, and $\delta^{13}\text{C}$ (CO₂) values of the groundwater volatiles reveal a mixture of mantle and deep crustal (metamorphic) fluid origins. The flux of fluids into the seismogenic zone at high hydrostatic pressure may cause fault rupture, and transfer volatiles into the shallow crust.

We calculate an upward fluid flow rate of 147 mm a⁻¹ along the SAFS, up to 37 times higher than previous estimates (Kennedy et al., 1997). However, using newly identified characteristics of the SAFS, we calculate a total flux of ³He along the SAFS of 7.4×10^3 cm³ STP a⁻¹ (0.33 mol ³He a⁻¹), and a CO₂ flux of 1.5×10^{13} cm³ STP a⁻¹ (6.6×10^8 mol a⁻¹), ~1% of previous estimates. Lower fluxes along the Big Bend section of the SAFS suggest that the flux of mantle volatiles alone is insufficient to cause the super hydrostatic pressure in the seismogenic zone; however, results identify crustal (metamorphic) fluids as a major component of the CO₂ volatile budget, which may represent the additional flux necessary for fault weakening pressure in the SAFS.

Published by Elsevier B.V.

1. Introduction

The San Andreas Fault System (SAFS) in California is the most active fault system in the continental USA. In the historical record, numerous high-magnitude earthquakes have resulted in displacement along the SAFS. In the central and southern sections, these include, in chronological order, the Fort Tejon (*M* = 7.9; 1857), Imperial Valley (*M* = 7.8; 1892; *M* = 7.1; 1940), San Francisco (*M* = 7.8; 1906), Loma Prieta (*M* = 6.9; 1989), Landers (Mojave) (*M* = 7.3; 1992), Northridge (*M* = 6.7; 1993), Hector Mine (Mojave) (*M* = 7.1; 1999), and Mexicali (*M* = 7.2; 2010) (U.S. Geological Survey, 2011) earthquakes. Nearly 30 million people live in close proximity to the SAFS and are at risk from earthquake-related damage. Understanding the timing and

mechanisms that lead to fault failure is essential for civil planning, and for a deeper understanding of tectonic processes.

One explanation for weakness along the SAFS is the reduction of the effective stress by fluid overpressure. Models that invoke elevated fluid pressure for fault-weakening propose several different fluid sources, including crustal metamorphic-derived and mantle-derived fluids. Some crustal-fluid models suggest the infiltration of fluids from the surrounding host rock, and subsequent compaction and thermal expansion of sealed fault-zone materials (Sleep and Blanpied, 1992; Byerlee, 1993) requiring that the base of the seismic zone, the brittle–ductile transition, to be an impermeable boundary. Others identify metamorphic alteration of the underlying Franciscan formation and local limestone compaction as the fluid sources (Pili et al., 2002, 2011) or combine mantle and crustal dehydration fluxes (Faulkner and Rutter, 2001). In these cases, the recurrent overpressure would require fluid recharge. The continuous mantle–fluid flux

* Corresponding author. Tel.: +1 619 225 6100.

E-mail address: kulongos@usgs.gov (J.T. Kulongoski).

model explains the increased pore pressure as a result of a vertical flux of deep crust or mantle fluids into the seismogenic zone (Barnes et al., 1984; Bredehoeft and Ingebritsen, 1990; Rice, 1992; Kennedy et al., 1997; Kharaka et al., 1999; Chiodini et al., 2011). The investigation of exhumed faulted rocks, vein fillings, and fluid inclusions (Pili et al., 2011) or fault-zone drill fluids (Wiersberg and Erzinger, 2011) offer promising approaches for investigating the origin, evolution, and flowpaths of the fluids.

The study of helium in earthquake-prone regions is of particular interest because helium isotope systematics in fluids is sensitive to mixing between crustal and mantle end members. Indeed, helium, when coupled with CO₂, also can be used to quantify mixing between crustal and mantle-derived volatiles in fluids, and to estimate mantle He and CO₂ fluxes, as shown by Kennedy et al. (1997) for the SAFS. In this vein, we report helium and CO₂ abundances and isotopic characteristics of groundwater collected at wells adjacent or close to the Big Bend section of the SAFS. Our aims are four-fold: (1) determine the origin of fluids, and calculate the mixing proportions between crustal and mantle volatile inputs, (2) estimate the absolute flux of CO₂ released to the surface via this section of the SAFS, (3) evaluate whether observed fluxes are sufficient to sustain pore-fluid pressure in the seismogenic zone at a level sufficient to cause fault weakening, and (4) explain the heterogeneity in helium isotope values in wells which are in close proximity to one another, as observed elsewhere along the SAFS (e.g. Kennedy et al., 1997).

2. Cuddy Mil Potrero, and Cuyama valleys, California

2.1. Tectonic environment

The ~1300-km-long San Andreas Fault System (SAFS) delineates the boundary between the North American and Pacific plates (Wallace, 1990). It began forming ~30 Ma – following a shift from subduction to transform motion, and the development of the northward-migrating Mendocino Triple Junction (Wallace, 1990). The relative motion between the North American and Pacific plates along the transform boundary over the past 3 to 4 million years has been estimated at ~50 mm a⁻¹, based on marine magnetic anomalies (DeMets et al., 1987), with a N 35° W direction of dextral slip between the plates. Geologic offset and geodetic data for the SAFS, on the other hand, suggest a slip rate between 7 and 43 mm a⁻¹ (Stirling et al., 1996), with a mean value of ~35 mm a⁻¹ (Hill et al., 1990), with the main fault trace striking N 65–70° W. This discrepancy in direction and slip rates can be accounted for by extensional deformation of the western margin of the North American Plate at 10 mm a⁻¹ in a N 56° W direction (Hill et al., 1990).

The last major earthquake along the central section of the SAFS, the 1857 Fort Tejon earthquake, resulted in a 300 km-long rupture from the Cholame Valley to Wrightwood (Sieh, 1978). The maximum fault displacement of ~9 m occurred in the Carrizo Plain section, with less slip occurring to the north and south. Crustal deformation measurements along the Carrizo Plain section of the SAFS indicate 30 mm a⁻¹ of right-lateral slip (Sieh, 1978).

The Cuyama, Mil Potrero, and Cuddy valleys lie within the seismically-active SAFS which, in this region, is dominated by northwest-trending, right lateral strike-slip faults. The Cuyama Valley is bounded to the north by the Morales Fault and to the west and south by the South Cuyama, Ozena, and Big Pine faults, all of which are associated with the SAFS.

2.2. Hydrogeology of the study area

The study area includes the Cuyama Valley, and to the east along the SAFS, the Mil Potrero and Cuddy valleys (Fig. 1). The primary water-bearing formations are mainly unconfined and are composed of younger (Holocene) and older (Pleistocene) alluvium (consisting

of alternating layers of sands, gravels, silts, and clays) (Mathany et al., 2009). The study area is bounded on the west and south by the Sierra Madre Mountains, on the south by Mount Pinos, Cerro Noroeste, and Sawmill Mountain, on the north by the Caliente Range and Tecuya Ridge, and to the east by the Tehachapi Mountains. Altitudes of land surface range from about 600 m in the Cuyama Valley to the west, to about 2688 m at Sawmill Mountain to the southeast. The groundwater basins are mostly Quaternary alluvial fill, while the surrounding mountains are Mesozoic granites, volcanics and sedimentary units (Mathany et al., 2009).

3. Field and laboratory methods

Groundwater samples were collected from 18 wells in the Cuyama, Cuddy, and Mil Potrero valleys of southern California (Fig. 1), from August to December 2008, as part of the Priority Basins Project of the Groundwater Ambient Monitoring and Assessment Program (<http://ca.water.usgs.gov/gama/>). The wells included 10 public supply wells, 5 domestic wells, and 3 irrigation wells with a median well depth of ~100 m (Mathany et al., 2009). Dissolved gas (helium and CO₂) samples were collected in 3/8 inch-diameter copper tubes (~35 cm long) using braided nylon tubing connected to a hose bib at the wellhead. Groundwater was flushed through the tubing to dislodge bubbles before the flow was restricted with a back-pressure valve. Refrigeration clamps on either end of the copper tube were then tightened, trapping a sample of groundwater for analyses of dissolved noble gases and CO₂ (e.g. Weiss, 1968; Kulongoski and Hilton, 2011).

At the Scripps Institution of Oceanography, samples were released into an ultra-high vacuum extraction line (Kulongoski and Hilton, 2002) where dissolved gases were exsolved from the water phase, aided by acidification to ensure complete release of dissolved CO₂. The CO₂ and He–Ne fractions were isolated from other gases, by a combination of active-gas gettering and/or cryogenic separation, and captured in glass breakseals for transfer to dedicated lines for further purification and manometric measurement. Isotopic analyses proceeded adopting analytical protocols described previously (Shaw et al., 2003; Kulongoski and Hilton, 2011). A fraction of the CO₂ gas was collected in a Pyrex glass tube, on which the δ¹³C values were measured using a Delta V isotope ratio mass spectrometer (Ray et al., 2009; Hilton et al., 2010). The international standard Pee Dee Belemnite (V-PDB) was used for calibration, and an overall precision of less than 0.1‰ was achieved. The accuracy of the δ¹³C determination (±0.5‰) was estimated by repeat analyses of a working laboratory standard, itself calibrated relative to V-PDB.

Noble gas samples were analyzed at the Lawrence Livermore National Laboratory (LLNL) using an isotope dilution protocol and VG-5400 mass spectrometer (Cey et al., 2008). Uncertainties were calculated as the highest of the following: (1) best typical precision for the parameter (2% for ³He/⁴He, He, and Ne contents); (2) reproducibility of concurrently run air standards; (3) propagated uncertainty of the unknown sample ratio (for ³He/⁴He analyses only, to account for instrumental variation in background ³He count rates).

4. Results

Results of the He analyses (isotope compositions and concentrations) are reported in Table 1. In addition, Ne concentrations are given, in order to correct for the presence of excess air-derived atmospheric helium, together with tritium (³H) contents of the water phase to assess possible contributions to the ³He inventory from the decay of atmospheric tritium generated in the 1960s by nuclear-weapons testing. Results of the CO₂ analyses (isotope compositions and concentrations) along with CO₂/³He molar ratios are reported in Table 2.

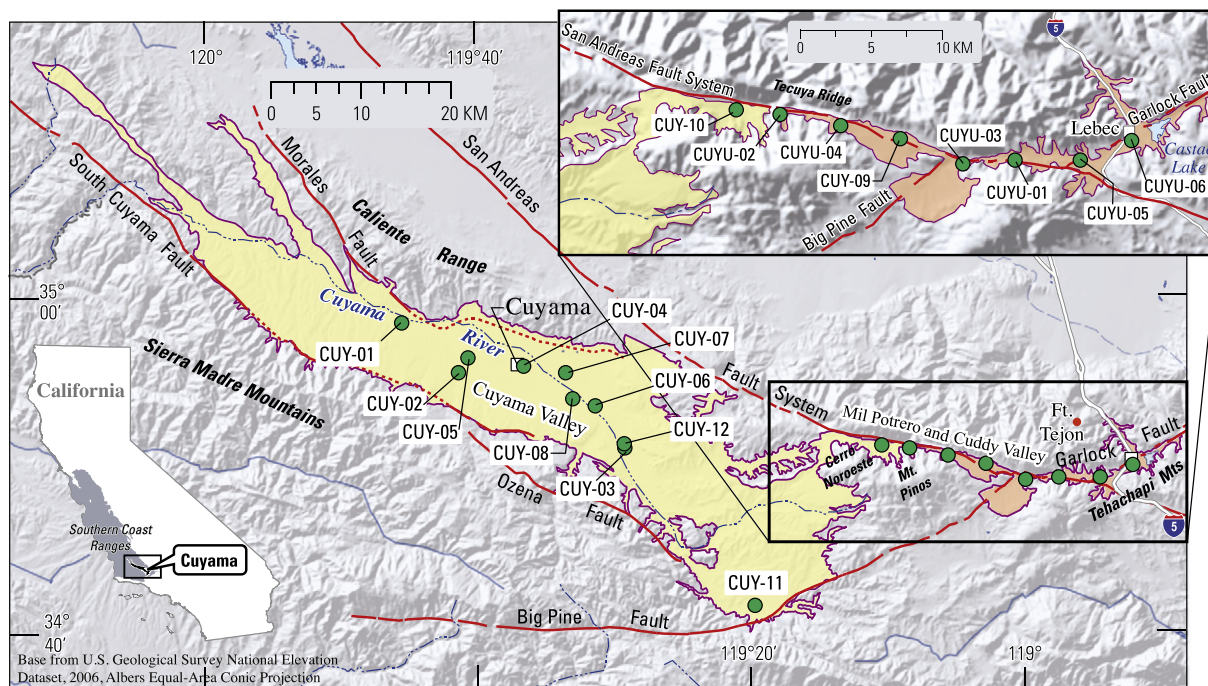


Fig. 1. Map of the Cuyama, Mil Potrero and Cuddy valleys along the Big Bend section of the San Andreas Fault System in California, USA. The locations of major faults, geographic features, and wells sampled in this study are shown.

4.1. Helium-4 concentrations

The helium concentrations presented in Table 1 have been corrected for excess air-derived helium (He_A) resulting from air-bubble entrainment. The excess-air component was calculated using measured 4He and Ne contents, and air-saturated water (ASW) equilibrium concentrations (He_{EQ} and Ne_{EQ}) at 15 °C – the assumed average annual recharge temperature for the samples (Torgersen, 1980; Kulongoski et al., 2008) – and the altitude at each well. Assuming that all Ne in a sample is of atmospheric origin, excess Ne (Ne_A), i.e. the amount greater than the equilibrium neon concentration at 15 °C (Ne_{EQ}), is multiplied by the atmospheric He/Ne ratio (0.288; Weiss, 1971) to derive He_A (Torgersen, 1980; Kulongoski et al., 2008). Therefore, corrected helium (He_C) concentrations reflect the measured sample He concentration minus He_A (Table 1). Here we note that a small amount of atmospheric helium (He_{EQ}) remains in He_C after the correction. Thus, atmospheric helium (He_{EQ}) is still present in the corrected $^3He/^4He$ ratios (R_C), however its influence is insignificant in high helium content samples, which are of primary interest in this study. Corrected concentrations (He_C) less than ASW values ($\sim 3.6\text{--}4 \times 10^{-8} \text{ cm}^3 \text{ STP g}^{-1} \text{ H}_2\text{O}$ at 15 °C; Weiss, 1971) reflect an overcorrection of He_A and, in these cases, it is assumed that He_C are entirely ASW concentrations (i.e. no extraneous helium). He_C range from $\sim 4 \times 10^{-8}$ (ASW values) to $62.7 \times 10^{-8} \text{ cm}^3 \text{ STP g}^{-1} \text{ H}_2\text{O}$, and He_A values range from 0.5 to $11.3 (\times 10^{-8}) \text{ cm}^3 \text{ STP g}^{-1} \text{ H}_2\text{O}$.

Groundwaters in the Mil Potrero and Cuddy valleys near the SAFS contain greater He_C concentrations (median $He_C = 20.2 \times 10^{-8} \text{ cm}^3 \text{ STP g}^{-1} \text{ H}_2\text{O}$) than samples from the Cuyama Valley (median $He_C = 4.80 \times 10^{-8} \text{ cm}^3 \text{ STP g}^{-1} \text{ H}_2\text{O}$) (Fig. 2a). The He_C concentrations are greater than expected for air-saturated water (3.64 to $3.99 \times 10^{-8} \text{ cm}^3 \text{ STP g}^{-1} \text{ H}_2\text{O}$; Weiss, 1971) at the altitudes of wells (1091–1840 m) in the Mil Potrero and Cuddy valleys. This observation is consistent with the addition of He from extraneous (non atmospheric) sources to all samples. However, in the Cuyama Valley, He_C concentrations for most samples are near ASW concentrations at the altitude of wells (582–840 m), (~ 4.1 to $4.3 \times 10^{-8} \text{ cm}^3 \text{ STP g}^{-1} \text{ H}_2\text{O}$; Weiss, 1971), and contain little or no extraneous helium.

4.2. $^3He/^4He$ ratios

The measured $^3He/^4He$ ratios of groundwater samples are corrected for air-derived excess He (He_A), tritiogenic helium-3 ($^3He_{TRIT}$) from the decay of nuclear-bomb derived tritium (Table 1), and normalized to the $^3He/^4He$ ratio of air ($R_A = 1.4 \times 10^{-6}$; Clarke et al., 1976), to determine whether groundwater is enriched in crustal ($0.02 R_A$; Andrews, 1985) and/or mantle ($8 R_A$; Graham, 2002) helium. Corrected $^3He/^4He$ ratios (R_C) range from 0.09 to $3.52 R_A$, consistent with mantle He constituting up to 43.9% of the total He in one sample. Note that the mantle $^3He/^4He$ ratio of $6 R_A$ may be more appropriate for subcontinental mantle (Dunai and Baur, 1995; Dunai and Porcelli, 2002), but $8 R_A$ was used in calculations in order to compare this work with that of Kennedy et al. (1997). The helium components in samples were calculated using a simple binary mixing model based on the measured $^3He/^4He$ ratio of the sample being composed of mantle ($8 R_A$) and crustal ($0.02 R_A$) end members. After correction for excess air and $^3He_{TRIT}$, most groundwater samples exhibit distinguishable mantle helium-3 contents. However, 4 groundwater samples from Cuyama Valley have helium concentrations near ASW, contain tritium, are thought to be recently recharged, and contain no mantle helium-3.

Notably, higher $^3He/^4He$ ratios are observed in wells near the SAFS in the Mil Potrero and Cuddy valleys (Fig. 2b). In a simple two component crust–mantle mixing model, the high R_C/R_A ratios represent a median mantle-derived He contribution of 21.7% in the wells along the SAFS, with CUYU-04 having 43.9% mantle He. Alternative explanations for high $^3He/^4He$ ratios, such as radioelement heterogeneity, high lithium contents, or fractionation processes, such as the preferential release of 3He from the aquifer matrix (Martel et al., 1990; Ballentine and Burnard, 2002), are highly unlikely based upon prior studies in the Mojave Desert section of the SAFS (Kulongoski et al., 2003, 2005).

It also is worth noting that in the Cuddy Valley, there is considerable spatial variability of the He isotopic ratios (and the helium concentrations) between wells within relatively close (~ 4 km) proximity to each other. For example, two of the highest values, $3.52 R_A$ and $2.30 R_A$ (from CUYU-04 and CUYU-02, respectively) are from wells in the Cuddy Valley near the SAFS (Table 1). However, a third site < 4 km

Table 1
Measured helium abundances and isotopic ratios, neon, and tritium abundances. Calculated helium-3 from tritium, corrected helium abundances and isotopic ratios, percent mantle helium, and distances of wells from faults in the Big Bend section groundwaters.

	Sample ID	Helium (cm^3 STP g^{-1} H_2O) ($\times 10^{-8}$)	($\pm 1 \sigma$)	$(^3\text{He}/^4\text{He})/R_A^a$ (1σ)	Neon (cm^3 STP g^{-1} H_2O) ($\times 10^{-8}$)	Tritium (pCi/L)	$^3\text{He}_{\text{TRIT}}^b$ (cm^3 STP g^{-1} H_2O) ($\times 10^{-14}$)	He_C ($\times 10^{-8}$)	(1σ)	$(^3\text{He}/^4\text{He})_C/R_A^a$ (1σ)	Percent mantle (%)	Distance from SAFS (km)	Distance from any fault (km)			
Cuyama Valley	CUY-01	6.53	± 0.13	0.78	± 0.01	19.7	2.9	2.27	6.03	± 0.38	0.50	± 0.02	6.1	17.7	1.43	
	CUY-02	12.65	± 0.25	0.40	± 0.01	24.2	0.0	0.0	10.80	± 0.51	0.30	± 0.02	3.5	16.9	4.19	
	CUY-03	16.73	± 0.33	0.97	± 0.03	56.8	7.2	5.63	5.38	± 1.10	0.20	± 0.06	2.3	11.9	3.11	
	CUY-04	5.64	± 0.11	0.93	± 0.03	45.5	0.9	0.70	4.19	± 0.86	1.00	± 0.06	0	11.9	3.09	
	CUY-05	9.13	± 0.18	0.52	± 0.02	20.9	0.0	0.0	8.23	± 0.43	0.47	± 0.04	5.6	15.5	4.00	
	CUY-06	6.05	± 0.12	1.04	± 0.02	25.1	6.6	5.16	4.15	± 0.48	1.00	± 0.04	0	10.0	5.89	
	CUY-07	5.05	± 0.10	1.02	± 0.03	24.4	4.3	3.36	4.17	± 0.72	1.00	± 0.06	0	9.5	2.75	
	CUY-08	6.91	± 0.14	1.17	± 0.04	29.8	9.0	7.04	4.16	± 0.88	1.00	± 0.08	0	11.2	5.43	
	CUY-11	6.29	± 0.13	0.82	± 0.02	21.7	2.5	1.96	4.89	± 0.42	0.49	± 0.04	6.0	21.0	1.90	
	CUY-12	13.20	± 0.26	0.94	± 0.02	46.9	6.3	4.92	4.70	± 0.91	0.09	± 0.04	0.9	11.4	3.49	
	Mil Potrero and Cuddy valleys	CUY-09	19.71	± 0.39	0.68	± 0.01	20.9	0.5	0.39	18.23	± 0.53	0.64	± 0.02	7.8	0.19	0.19
		CUY-10	41.01	± 0.82	3.00	± 0.03	25.2	2.8	2.19	38.32	± 0.89	3.10	± 0.06	38.6	0.58	0.19
CUYU-01		12.52	± 0.25	1.62	± 0.03	22.1	7.4	5.79	10.82	± 0.48	1.33	± 0.06	16.5	0.13	0.13	
CUYU-02		23.86	± 0.48	2.40	± 0.04	22.0	8.4	6.57	22.12	± 0.61	2.30	± 0.08	28.6	0.28	0.28	
CUYU-03		71.61	1.43	2.07	± 0.03	46.8	6.8	5.32	62.74	± 1.58	2.16	± 0.06	26.9	0.10	0.10	
CUYU-04		53.24	± 1.06	3.47	± 0.05	22.7	4.4	3.44	51.15	± 1.10	3.52	± 0.10	43.9	0.29	0.29	
CUYU-05		7.64	± 0.15	0.93	± 0.01	26.0	7.1	5.52	4.95	± 0.59	0.10	± 0.02	1.1	0.84	0.17	
CUYU-05 replicate		6.73	± 0.13	0.89	± 0.01	22.3	7.4	5.79	5.10	± 0.54	0.05	± 0.02	0.4	–	–	
CUYU-06	16.18	± 0.32	1.27	± 0.01	35.3	7.4	5.79	10.89	± 0.72	1.02	± 0.02	12.6	3.6	0.40		
CUYU-06 replicate	21.43	± 0.43	1.27	± 0.01	42.4	7.4	5.79	14.10	± 1.29	1.12	± 0.02	13.9	–	–		

^a R_A is the $^3\text{He}/^4\text{He}$ ratio of air, 1.4×10^{-6} .

^b Calculated from the measured ^3H extrapolated to 1967 ^3H and decayed to 2008 $^3\text{He}_{\text{TRIT}}$.

Table 2
Carbon dioxide abundances, carbon isotopes, CO₂/³He_c ratios, and calculated ternary mixing components based on CO₂/³He_c and δ¹³C of Big Bend section groundwaters.

Sample ID	CO ₂ (cm ³ STP g ⁻¹ H ₂ O) (1 σ)	CO ₂ / ³ He _c (×10 ¹¹)	δ ¹³ C (‰) (1 σ)	Limestone (L)	Organic carbon (S)	Mantle (M)	Limestone (L)	Organic carbon (S)	Mantle (M)
				0‰	–30‰ (percent)	–6.5‰	0‰	–22‰ (percent)	–6.5‰
Cuyama Valley	0.108 ± 0.002	25.64	–13.75 ± 0.05	54.1	45.8	0.1	37.4	62.5	0.1
	0.059 ± 0.001	11.01	–17.14 ± 0.04	42.7	57.1	0.2	22.0	77.9	0.2
	0.109 ± 0.002	18.72	–21.50 ± 0.04	28.3	71.7	0.0	2.2	97.7	0.1
	0.076 ± 0.002	22.57	–19.32 ± 0.04	35.5	64.4	0.1	12.1	87.8	0.1
	0.084 ± 0.002	141.9	–12.18 ± 0.03	59.4	40.6	0.02	44.6	55.4	0.01
Mil Potrero and Cuddy valleys	0.124 ± 0.002	0.746	–20.24 ± 0.05	30.4	66.9	2.7	6.1	91.2	2.7
	0.179 ± 0.004	8.85	–12.89 ± 0.05	56.9	42.9	0.2	41.3	58.5	0.2
	0.223 ± 0.005	3.13	–12.44 ± 0.04	58.0	41.3	0.6	43.0	56.4	0.6
	0.194 ± 0.004	1.023	–13.41 ± 0.04	53.8	44.3	2.0	37.7	60.4	2.0
	0.193 ± 0.004	–	–13.81 ± 0.06	–	–	–	–	–	–
	0.155 ± 0.003	0.614	–11.87 ± 0.05	57.9	38.9	3.3	43.8	53.0	3.3

away has a value (0.64 R_A) that is 5 times lower than the well with the highest value (Fig. 1). The implications of such spatial heterogeneity in ³He/⁴He values are discussed in Section 5.1.

4.3. CO₂ concentrations and carbon isotopes

Carbon dioxide concentrations in the 10 wells sampled range from 0.059 to 0.223 cm³ STP g⁻¹ H₂O. The highest CO₂ concentrations are found in wells near the SAFS, in the Mil Potrero and Cuddy valleys (Table 1), and contain significantly higher concentrations of CO₂ (median of 0.18 cm³ STP g⁻¹ H₂O) than the Cuyama Valley samples (median of 0.084 cm³ STP g⁻¹ H₂O), which are near associated faults (Fig. 2c). The δ¹³C (CO₂) values measured in 10 groundwater samples range from –21.5 to –11.9‰ (vs. PDB) (Table 1). All values are less than the average mantle range (–6.5 ± 2‰; Pineau et al., 1976; Pineau and Javoy, 1983; Sano and Marty, 1995). The wells in Mil Potrero and Cuddy valleys along the SAFS have greater δ¹³C values (median of –12.9‰) than the wells in the Cuyama Valley (median of –17.1‰) (Table 2; Fig. 2d).

4.4. CO₂/³He ratios

The CO₂/³He values in the samples range from 0.614 to 141.9 (×10¹¹) (Table 2). The groundwater CO₂/³He ratios (He corrected for air entrainment) are intermediate between values considered typical for mantle-derived CO₂-rich (2 ± 1 × 10⁹; Marty and Jambon, 1987) and crustal-derived (10¹¹ to 10¹⁴) volatiles (O'Nions and Oxburgh, 1988). CO₂/³He values are considerably lower in samples along the SAFS from the Mil Potrero and Cuddy valleys (median = 1.02 × 10¹¹), than in the samples from the Cuyama Valley (median = 22.6 × 10¹¹). However, gases with a substantial mantle helium component exhibit a range in CO₂/³He values – overlapping crustal values – and, as such, CO₂/³He values alone cannot identify mantle-derived carbon (O'Nions and Oxburgh, 1988). Thus it is necessary to consider the CO₂, ³He/⁴He, and δ¹³C (CO₂) characteristics of the volatiles together (Table 2).

5. Discussion

The following sections discuss the distribution and provenance of helium and CO₂ measured in samples from the Cuyama, Mil Potrero and Cuddy valleys, and the processes that control the He–CO₂ systematics of fluids associated with the SAFS.

In Section 5.1, helium sources and mixing relationships are discussed, while in Section 5.2 contributions to total CO₂ are estimated based on the He–CO₂ and δ¹³C (CO₂) characteristics of the samples. In Section 5.3, the upward flow of fluids along the SAFS, the flux of helium, and the flux of CO₂ are estimated. Finally, in Section 5.4,

fault weakening models and the role of faults in the transport of mantle volatiles are discussed.

5.1. Distribution of mantle-derived helium near the SAFS

The highest ³He/⁴He ratio, 3.52 R_A (~44% mantle contribution), was measured in a well along the SAFS in the Cuddy Valley (Table 1). The well, CUYU-04, is ~290 m from the SAFS. Fig. 2a and b show the plots of He_c and R_c/R_A versus distance of all wells from the fault. The distribution of the He data shows that 6 of the 8 groundwater samples collected near the SAFS have higher ³He/⁴He and He_c than the groundwaters in the Cuyama Valley, which is bounded by the associated Morales, Ozena, South Cuyama, and Big Pine faults (Fig. 1). The median ³He/⁴He in the Mil Potrero and Cuddy valleys is 1.75 R_A , while in the Cuyama Valley, the median value is 0.5 R_A , corresponding to mantle-He contributions of 21.7% and 6.1%, respectively. This suggests a much larger mantle-He contribution in wells along the SAFS, and provides evidence for the enhanced transfer of mantle volatiles through the SAFS. Interestingly, the 10 wells in Cuyama Valley lie within 0.3–5.8 km of other identified faults (Fig. 1); however, the ³He/⁴He values of these samples range from 0.09 to 1.0 R_A . These 10 wells contain 0 to 6.1% mantle He. While the flux of mantle volatiles appears to be focused along the SAFS, adjacent faults also appear to facilitate the transfer of mantle volatiles through the crust albeit to a lesser extent.

Wells located within 1 km of the SAFS display a surprising spatial variability in ³He/⁴He. Several mechanisms may explain this observation, including variability in the amount of mixing with crustal He which acts to dilute the mantle He component. A plot of R_c/R_A vs. He_c (Fig. 3) shows a general increase in ³He/⁴He with an increase in He_c for the Mil Potrero and Cuddy valley samples indicating that enhanced input of helium into these groundwaters is predominantly a result of an increase in the mantle-derived component. Conversely, the Cuyama Valley wells show a decrease in ³He/⁴He with an increase in He_c, indicating that this flow system is dominated by crustal-helium addition.

Other processes that explain spatial variability of ³He/⁴He ratios observed in wells located within close proximity include (1) heterogeneous local lithologies (Torgersen, 1980), (2) focused flow of helium-rich groundwater as a consequence of sub-regional flow cells in the aquifer (Bethke et al., 2000), and (3) fracturing and the time-dependent hydraulic transport of the He-rich fluids through the crust (Nur and Walder, 1990). This last explanation could effectively transfer mantle helium to the proximal pore-fluid or release crustal He from the aquifer lithology (Torgersen and O'Donnell, 1991).

The alluvial basins sampled for this study have similar lithologies composed of Quaternary alluvial fill, and are not large enough for

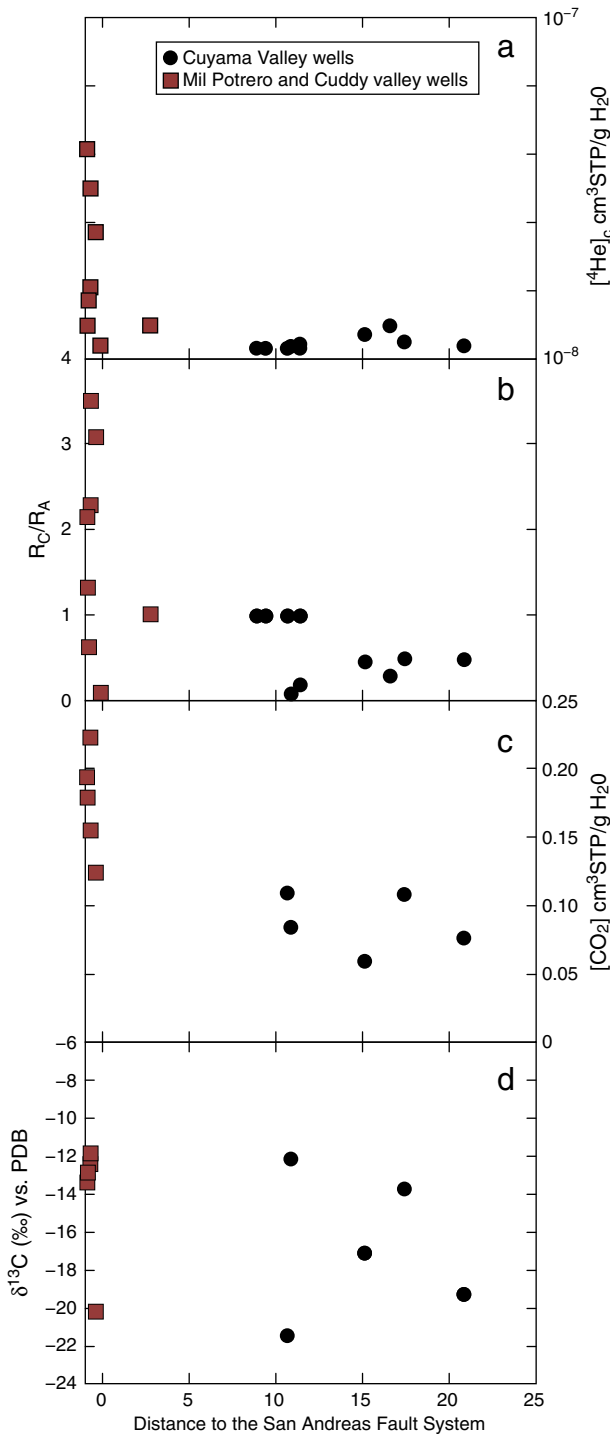


Fig. 2. (a) Plot of helium corrected for air-bubble entrapment (He_c); (b) Helium isotope ratios corrected for air-bubble entrapment normalized to the $^3He/^4He$ ratio of air (R_A); (c) measured carbon dioxide (CO_2); (d) and carbon isotopes ($\delta^{13}C$) of (CO_2), versus the distance of the well from the San Andreas Fault System (SAFS). Groundwater samples from the Mil Potrero and Cuddy valleys (red squares) are closest to the SAFS and generally have higher helium abundance and isotope ratios, and carbon dioxide abundance and isotope ratios than samples from the Cuyama Valley (black circles).

long, sub-regional flow-cells. However, episodic faulting and fracturing could release accumulated radiogenic He on geologically-short time-scales (~1500 years) (Torgersen and O'Donnell, 1991), or enhance the transfer of mantle volatiles through permeable fault

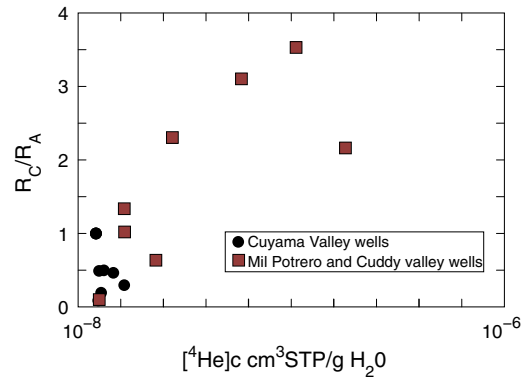


Fig. 3. Plot of helium isotope ratios corrected for air-bubble entrapment normalized to the $^3He/^4He$ ratio of air (R_A) versus helium corrected for air-bubble entrapment (He_c). Groundwater samples from the Mil Potrero and Cuddy valleys trend towards higher R_C/R_A values with greater He_c , while samples from the Cuyama Valley decrease with increasing He_c .

zones (Nur and Walder, 1990; Kulongoski et al., 2005), such that subsequent proximal fluid flow could then explain variations in He fluxes. This possibility would explain the marked variability in He values in the basins along the SAFS. Recent work on drilling mud gas at the San Andreas Fault Observatory at Depth (SAFOD) shows variation, at small scales, in the helium isotope composition at seismogenic depths of the SAF suggesting that variations in fluid flow rates from depth due to permeability differences explains the observed variations in $^3He/^4He$ (Wiersberg and Erzinger, 2011). These authors also concluded that the principal pathway for mantle volatiles is through permeable country rock of the North American Plate (Wiersberg and Erzinger, 2011).

The difference in $^3He/^4He$ between the Mil Potrero and Cuddy valleys, and the Cuyama Valley, could be related to differences in local geology. Although all of the wells sampled are drilled in Quaternary alluvium deposits, the Mil Potrero and Cuddy valleys are surrounded by Precambrian metamorphic and Mesozoic granitic plutons, while the Cuyama Valley is surrounded by uplifted Cenozoic, Miocene and Eocene marine sediments (California Division of Mines and Geology, 2000). However, no evidence exists for recent volcanic eruptions in either of these areas. Past volcanism and magmatism are associated with the northward development of the SAFS from 30 to 8 Ma ago (Wallace, 1990). During emplacement and eruption, magma degasses, enriching the nearby hydrologic system in 3He and 4He . However, over the course of 8–30 Ma, the in-growth of crustal 4He in host aquifer rocks will act to mask these elevated $^3He/^4He$ ratios (Kennedy et al., 1997). As such, older plutonic and volcanic rocks are not expected to be significant sources of contemporary high $^3He/^4He$ ratios.

Alternatively, the distribution of elevated $^3He/^4He$ ratios could result from the transport of helium, exsolved from incipient upper mantle melts, through the SAFS to the shallow crust (Kennedy et al., 1997; Kharaka et al., 1999; Kulongoski et al., 2003, 2005) or from dehydrated serpentinitized Franciscan mantle wedge (Fulton and Saffer, 2009). In the first case, as mantle helium (~8 R_A) is transferred through the crust, it mixes with crustal helium (~0.02 R_A), thereby lowering the resultant $^3He/^4He$ ratio to values determined by the rate of transfer, or residence time of fluids in the crust (Kennedy et al., 1997). In the later case, fluids derived from Franciscan rocks could have elevated helium isotope ratios, and observed helium ratios could be explained by serpentinite degassing (Wiersberg and Erzinger, 2011). The continuous transport of mantle volatiles into the seismogenic zone of the SAF is a more probable explanation for elevated $^3He/^4He$ ratios due to low diffusivity of He in solid rock (~5 × 10⁻⁷; Ballentine and Burnard, 2002; Kulongoski et al., 2005; Wiersberg and Erzinger, 2011). Flow rates of mantle-derived fluids are estimated in Sections 5.3 and 5.4.

5.2. CO₂ provenance and He–CO₂ characteristics along the SAFS

The highest CO₂ concentrations in groundwater samples are measured in wells along the main trace of the SAFS in the Mil Potrero and Cuddy valleys (Fig. 2c). The highest concentration of CO₂ (0.223 cm³STP g⁻¹ H₂O) was measured at CUYU-02 in the Mil Potrero Valley, which is ~280 m from the SAFS. The median CO₂ concentration for the Mil Potrero and Cuddy valleys is 0.18 cm³ STP g⁻¹ H₂O, while in the Cuyama Valley, the median CO₂ concentration, 0.08 cm³ STP g⁻¹ H₂O, is less than half that value.

The isotopic composition of CO₂ (δ¹³C) has been used in many studies to identify CO₂ origin (e.g. Deines et al., 1974; Pineau et al., 1976; Pineau and Javoy, 1983; Schoell, 1983; Javoy et al., 1986; Whiticar, 1994; Baker et al., 1995; Wycherley et al., 1999). Characteristic mantle δ¹³C (CO₂) values range from -9 to -4‰ with an average of -6.5 ± 2.5‰, while organic CO₂ has δ¹³C values from -40 to -20‰, and marine carbonates have δ¹³C values ranging from -2 to +2‰. Sample δ¹³C (CO₂) values in this study fall between -21.5 and -11.9‰ indicating a mixture between organic (sedimentary) CO₂ and one or both of the other two components.

Four out of five samples located along the sections of the SAFS in the Cuddy and Mil Potrero valleys have δ¹³C > -13.4‰. The site with the highest δ¹³C value (-11.9‰, CUYU-04) is also the well with the highest ³He/⁴He value (3.52 R_A), however these four sites have fairly constant δ¹³C values with increasing helium concentrations. Two of the five sites in the Cuyama Valley have relatively elevated δ¹³C (-13.8 and -12.2‰), while the other three sites have values < -17.1‰, all of which vary with helium concentration.

Mantle CO₂ is thought to act as a carrier gas that transports He to the Earth's surface because observed He and CO₂ in mantle fluids occur at near constant proportions to each other (Marty and Jambon, 1987; O'Nions and Oxburgh, 1988). At locations dominated by mantle input ("M"), fluids contain volatiles with CO₂/³He ratios near 2 × 10⁹ (Marty and Jambon, 1987). In crustal fluids, CO₂/³He ratios vary over a range of values (10⁸ to 10¹⁴) as a result of the addition of CO₂ from marine carbonates (limestone "L"; CO₂/³He = 1 × 10¹³) or organic-carbon rich sediments ("S"; CO₂/³He = 1 × 10¹³), or CO₂ loss through reaction or precipitation (O'Nions and Oxburgh, 1988). In general, CO₂/³He values greater than ~10¹¹ can be attributed to a crustal CO₂ source containing virtually no ³He.

Given that volatiles from the crust and mantle have distinctive ³He/⁴He, CO₂/³He, and δ¹³C (CO₂) values, these properties may be used to identify and quantify contributions from these two end members. A plot of CO₂/³He versus δ¹³C (Fig. 4) shows the distribution of samples in relation to the three major end members, M, L, and S, as

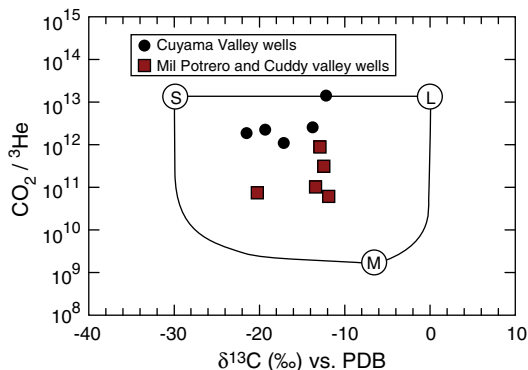


Fig. 4. ³He–CO₂–δ¹³C systematics: plot of CO₂/³He ratios versus δ¹³C values. Included are the end member values for the mantle (M), organic-rich carbon sediments (S), and marine carbonates-limestone (L). All groundwater samples plot between the end members suggesting mixing between volatile sources; however, the samples from the Mil Potrero and Cuddy valleys have lower CO₂/³He ratios suggesting a greater mantle influence than samples from the Cuddy Valley.

defined above. CO₂/³He values for wells in the Mil Potrero and Cuddy valleys range from 6.14 to 88.5 (× 10¹⁰). In the Cuyama Valley, CO₂/³He values range from 110 to 1419 (× 10¹⁰), closer to crustal CO₂/³He values (10¹¹ to 10¹³; Ballentine et al., 2002).

The proportion of CO₂ derived from each of the three end members (M, L and S) can be calculated using the CO₂/³He ratio and the δ¹³C for each sample following the approach of Sano and Marty (1995) – see Table 2 – and assuming that CO₂ and He are unfractionated from one another. The mantle δ¹³C value of -6.5‰, the marine carbonate (limestone) value of 0‰, and the sediment (organic carbon) δ¹³C value of -22‰ were used in the calculations. Selection of the sediment (organic carbon) δ¹³C value of -22‰ was based on previous estimates for the SAFS (Wiersberg and Erzinger, 2008). For comparison, the typical sediment (organic carbon) δ¹³C value of -30‰ was also used (Table 2). Crustal additions have affected each sample to a greater or lesser degree. Sediments (organic carbon -δ¹³C = -22‰) comprise the majority of the inputs to the CO₂ inventory of the samples, with mantle proportions ranging from 0.01 to 3.3%. This agrees with previous investigations that attributed the source of SAFS fluids primarily to metamorphism of organic-rich shale as the major source of CO₂ (Wiersberg and Erzinger, 2011). All 5 samples from the Cuyama Valley had <0.2% mantle CO₂. Note that the entrainment of atmospheric air bubbles, which have a δ¹³C value of -8.9‰ (Lewicki et al., 2003), could impact CO₂ systematics in young groundwater, but the low concentration of CO₂ in air makes this an extremely unlikely possibility.

In Fig. 5, the CO₂/³He ratios of samples are plotted versus corresponding ³He/⁴He ratios (R_C/R_A) to discern mantle and crustal contributions to each sample. Superimposed on the plot is the 'best fit' binary mixing curve, which represents the mixture of mantle and crustal volatiles with CO₂/³He ratios of 2 × 10⁹ and ~5 × 10¹³, respectively. The Mil Potrero, Cuddy, and Cuyama valley samples fall close to the same binary mixing curve. This is significant for two reasons: (1) the same two end member compositions are applicable for all samples in the Big Bend region, with Cuyama Valley samples having a greater crustal contribution, and (2) the CO₂/³He composition of the mantle end member, ~2 × 10⁹, is consistent with the value characteristic of MORB-type mantle. This latter point is important for estimating the flux of CO₂ (Section 5.3).

The high concentrations of CO₂ in the wells along the SAFS, relatively high δ¹³C values, and larger proportion of mantle-derived CO₂ (Mil Potrero and Cuddy valleys) parallel the trend of high ³He/⁴He close to the SAFS. Taken together, these observations provide further evidence that the SAFS is the focus of mantle degassing within the Big Bend section.

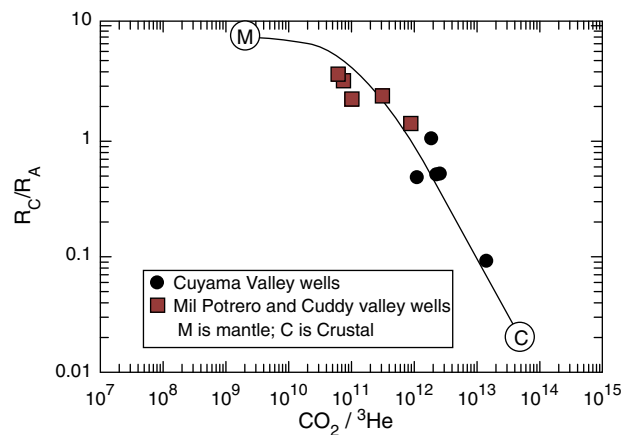


Fig. 5. Plot of helium isotope ratios corrected for air-bubble entrainment normalized to the ³He/⁴He ratio of air (R_A) versus CO₂/³He ratios. Included are mantle (M) and crustal (C) end member values and a 'best fit' binary mixing curve which represents the mixture of mantle and crustal volatiles with CO₂/³He ratios of 2 × 10⁹ and ~5 × 10¹³, respectively. All groundwater samples fall close to the same binary mixing curve, but the Mil Potrero and Cuddy valleys have a greater mantle contribution, while the Cuyama Valley samples have a greater crustal volatile contribution.

Table 3
Helium-3 and CO₂ flux characteristics from selected groundwater studies.

Crustal thickness (km)	System	Upward fluid flow rate (mm a ⁻¹)	Location	Local ³ He flux (mol cm ⁻² a ⁻¹) (×10 ⁻¹⁵)	Total ³ He flux (mol a ⁻¹)	CO ₂ flux (mol a ⁻¹) (×10 ¹⁰)	Reference
30	SAFS	147	Mil Potrero Valley, USA	1.7	5.8	5.8	This work ^a
30	SAFS	147	Mil Potrero Valley, USA	1.7	0.3	0.07	This work ^b
30	SAFS	4.0	Varian Phillips well, USA	1.8	6.3	6.3	Kennedy et al. (1997) ^a
30	SAFS	1.7	Mojave Desert, USA	0.09	0.02	0.004	Kulongoski et al. (2005) ^b
38	NAFZ	8.7	Mudurnu, Turkey	3.94	–	–	de Leeuw et al. (2010)
–	Non volcanic	–	Colorado Plateau, USA	–	–	0.14	Crossey et al. (2009)
–	Non volcanic	–	Central Italy	–	–	10.0	Rogie et al. (2000)
–	Arc volcano	–	Global arc volcanoes	–	–	160.0	Hilton et al. (2002)
–	Arc volcano	–	Global arc volcanoes	–	3–150	10–50	Marty et al. (1989)
–	Arc volcano	–	Global arc volcanoes	–	70	–	Allard (1992)
–	Global flux	–	Global flux	–	1500	–	Allard (1992)

^a Calculated with the parameters: CO₂/³He = 10¹⁰ and SAFS width 350 km.

^b Calculated with the parameters: CO₂/³He = 2 × 10⁹ and SAFS width 20 km.

5.3. Calculating SAFS volatile fluxes

Kennedy et al. (1997) calculated upward fluid flow rates through the SAFS assuming that as mantle fluids traverse the SAFS, locally produced crustal ⁴He dilutes mantle-like ³He/⁴He ratios, generating a vertical gradient in ³He/⁴He. This vertical gradient in helium isotopes depends on the upward flow rate and the crustal (radiogenic) production rate of ⁴He. Based on a 30 km crustal thickness (H_c), and the composition of the Varian–Phillips well located ~350 km north-west of Cuddy Valley near Parkfield, California (air-corrected mantle-He concentration: $He_{F,m} = 426.0 \times 10^{-7} \text{ cm}^3 \text{ STP g}^{-1} \text{ fluid}$, and ${}^3\text{He}/{}^4\text{He} = 2 R_A$), Kennedy et al. (1997) calculated an upward flow rate (q) of ~3 mm a⁻¹ at this well (Eq. (1)), with the caveat that flow rates could be considerably higher if flow is episodic.

$$q = \frac{H_c \rho_s P(\text{He})}{\rho_f [\text{He}]_{F,m}} \times \left[\frac{R_s - R_c}{R_m - R_s} \right] \quad (1)$$

In Eq. (1), ρ_s and ρ_f are the densities of the solid and fluid phases, $P(\text{He})$ is the present-day production rate from the U + Th in the fault zone materials, and R is the ³He/⁴He ratio of the (s) sample, (c) crust, and (m) mantle. In the Kennedy et al. (1997) study, fluid flow rates at different wells ranged between 1 and 10.5 mm a⁻¹, with the highest value derived for Mercy Hot springs, with a ratio of 4 R_A .

Using the same model, we calculate an upward fluid flow rate through the Big Bend section of the SAFS of ~147 mm a⁻¹, based on a 30 km crustal thickness, ⁴He production value ($P(\text{He})$) of $5.01 \times 10^{-13} \text{ cm}^3 \text{ STP g}^{-1} \text{ a}^{-1}$ (U = 2.3 ppm; Th = 7.9 ppm; Kulongoski et al., 2005), bulk rock density (ρ_s) of 2.8 g cm⁻³, the air-corrected mantle He concentration in CUYU-04, $He_{F,m} = 2.25 \times 10^{-7} \text{ cm}^3 \text{ STP g}^{-1} \text{ fluid}$, and sample $R_s = {}^3\text{He}/{}^4\text{He}_C = 3.52 R_A$. For comparison, the estimated upward fluid flux of site CUY-10, with the second highest ${}^3\text{He}/{}^4\text{He}_C = 3.10 R_A$, is 179 mm a⁻¹. In the nearby Mojave Desert, an upward fluid flux of 1.7 mm a⁻¹ was calculated for site 3N/8E-31J1 ($He_{F,m} = 10.3 \times 10^{-7}$; ${}^3\text{He}/{}^4\text{He} = 0.34 R_A$) (Kulongoski et al., 2005). In Turkey, along the North Anatolia Fault System (NAFS), de Leeuw et al. (2010) calculated an upward fluid flow rate of ~8.7 mm a⁻¹, based on a 38-km crustal thickness, ⁴He production value of $4.75 \times 10^{-13} \text{ cm}^3 \text{ STP g}^{-1} \text{ a}^{-1}$, a bulk rock density of 2.8 g cm⁻³, the mantle helium concentration at the Mudurnu well, $He_{F,m} = 20.1 \times 10^{-7} \text{ cm}^3 \text{ STP g}^{-1} \text{ fluid}$, and ${}^3\text{He}/{}^4\text{He} = 2.15 R_A$. Results from these studies are presented in Table 3. The upward flow rate calculated in Cuddy Valley is up to 37 times greater than the values calculated by Kennedy et al. (1997) and de Leeuw et al. (2010). The greater flux along this section of the SAFS primarily reflects the relatively high ³He/⁴He ratios and low mantle He abundances observed in the wells sampled for this study. As such, this study identifies one of the first locations where high mantle-helium concentrations

have been observed in relatively young, tritium-rich groundwater that has not accumulated significant quantities of radiogenic helium. A lower flux was estimated for the SAFS in the Mojave (Table 3); however, Mojave groundwater has low ³He/⁴He ratios, long groundwater residence times (>10,000 years), and high radiogenic (crustal) He concentrations (Kulongoski et al., 2005).

Fluids with high ³He/⁴He ratios likely indicate rapid transport of mantle volatiles to the shallow crust. Higher fluid flow may reflect greater permeability of the crust, which may result from local fault behavior. Evaluating the hypothesis that lower effective stress on the fault zone, allowing greater permeability, and as a result, varying flux rates for mantle volatiles is discussed in the next section.

5.4. Fault weakening models

The transfer of mantle volatiles across the brittle–ductile transition requires that this boundary is permeable and that fluids enter the seismogenic zone at or near lithostatic pressure (Kennedy et al., 1997). As such, it is possible to assess the impact of flow rate on the pressurization of the fault zone by calculating the total volatile flux. Kennedy et al. (1997) assumed a flow rate of 4 mm a⁻¹ for the SAFS, corresponding to a ³He flux through the SAFS of $\sim 4.05 \times 10^{-11} \text{ cm}^3 \text{ STP cm}^{-2} \text{ a}^{-1}$ ($\sim 2 \times 10^{-15} \text{ mol cm}^{-2} \text{ a}^{-1}$) (Eq. (2)).

$$\text{total } {}^3\text{He flux} = q \times \rho_f \times [\text{He}_s] \times R_s \quad (2)$$

In Eq. (2), q is upward fluid flux, ρ_f is the density of the fluid (~1 g cm⁻³), $[\text{He}_s]$ is the helium-4 concentration of the sample, R_s is the ³He/⁴He ratio of the sample. Integrating this flux over the entire network of faults that make up the SAFS (length = 1000 km; width = 350 km), Kennedy et al. (1997) derived a total flux of ³He of $1.42 \times 10^5 \text{ cm}^3 \text{ STP a}^{-1}$ (~6 mol a⁻¹). In this work, using the same parameters as Kennedy et al. (1997), we calculate an upward fluid flow of 147 mm a⁻¹ (Section 5.3), which corresponds to a total ³He flux of $3.7 \times 10^{-11} \text{ cm}^3 \text{ STP cm}^{-2} \text{ a}^{-1}$ ($1.7 \times 10^{-15} \text{ mol cm}^{-2} \text{ a}^{-1}$) adopting $R_s = 3.52$ and $[\text{He}_s] = 51 \times 10^{-8} \text{ cm}^3 \text{ STP g}^{-1} \text{ fluid}$ (CUYU-04; Table 1). If this value is applicable to the entire SAFS, and we adopt the same dimensions for the SAFS (1000-km-long by 350 km wide; Kennedy et al., 1997), then we calculate the total ³He flux through the SAFS to be $1.3 \times 10^5 \text{ cm}^3 \text{ STP a}^{-1}$ (5.8 mol ³He a⁻¹; Table 3) – similar to the estimate by Kennedy et al. (1997). However, this work has shown that the mantle-He signal is spatially restricted, to within ~10 km of the fault trace, i.e. ³He/⁴He ratios decrease rapidly with increasing distance from the SAFS (Fig. 3). Thus, for the above calculation we reduce the width of the actively degassing region from 350 km to 20 km (10 km either side of the fault trace), and this yields a revised total ³He flux of $7.4 \times 10^3 \text{ cm}^3 \text{ STP a}^{-1}$ (0.33 mol ³He a⁻¹), over an order of magnitude

less than the previous estimate (Table 3). For sample CUYU-4 (Cuddy Valley), the mantle-fraction of the helium-3 (e.g., calculated using the following equation from Aeschbach-Hertig (2005)):

$$\text{mantle fraction of } ^3\text{He} = \left[\frac{R_s - R_c}{R_m - R_s} \right] \times \frac{R_m}{R_s} \quad (3)$$

is 99.8%, thus the total ^3He flux is essentially the ^3He -mantle flux. For comparison, this revised SAFS flux is significantly larger than estimates for the Mojave Desert section of the SAFS ($0.02 \text{ mol } ^3\text{He a}^{-1}$; Table 3), however, it is 1–2 orders of magnitude lower than fluxes from arc volcanoes ($3\text{--}150 \text{ mol } ^3\text{He a}^{-1}$; Marty et al., 1989); ($70 \text{ mol } ^3\text{He a}^{-1}$; Allard, 1992) and virtually insignificant on a global scale ($1\text{--}1.5 \times 10^3 \text{ mol } ^3\text{He a}^{-1}$; Allard, 1992) (Table 3).

The calculated ^3He -mantle flux for the SAFS can be combined with a mantle $\text{CO}_2/{}^3\text{He}$ ratio of $\sim 2 \times 10^9$ (Marty and Jambon, 1987) (and see Fig. 5), and a 20-km-wide SAFS, to give a calculated mantle CO_2 flux of $1.5 \times 10^{13} \text{ cm}^3 \text{ STP a}^{-1}$ ($6.6 \times 10^8 \text{ mol a}^{-1}$), which is $\sim 1\%$ of the estimate by Kennedy et al. (1997) of $6.3 \times 10^{10} \text{ mol CO}_2 \text{ a}^{-1}$. However, the CO_2 flux through the SAFS is likely much greater, given that the mantle- CO_2 component comprises only up to 3.3% of the total CO_2 in the groundwater samples while metamorphic crustal volatiles contribute significantly (see Section 5.2). In comparison, the total non-volcanic flux estimated for central Italy is $\sim 10^{11} \text{ mol CO}_2 \text{ a}^{-1}$ (Rogie et al., 2000), and that of the Colorado Plateau is $\sim 1.4 \times 10^9 \text{ mol CO}_2 \text{ a}^{-1}$ (Crossey et al., 2009). Thus, the estimate from this work is $\sim 0.04\%$ of the total volcanic arc flux estimate of $1.6 \times 10^{12} \text{ mol CO}_2 \text{ a}^{-1}$ (Hilton et al., 2002) (Table 3).

Kennedy et al. (1997) argued that since the density and viscosity of CO_2 are comparable to water at seismogenic depths ($\sim 11\text{--}20 \text{ km}$ depth for the southern section of the SAFS; Smith-Konter et al., 2011), their reported CO_2 flux into the fault zone could generate the high pore pressures needed for fault weakening. However, this conclusion depends on the permeability of the lower crust, which is unknown. Assuming a constant permeability (and a porosity of 0.01 and rock compressibility of 10^{-4} MPa^{-1}), Kennedy et al. (1997) estimated that the ^3He -calculated CO_2 flux implies a fault zone permeability of 10^{-21} m^2 , and by assuming that permeability decreases exponentially with depth at a rate scaled to a linear increase in stress, fault zone permeability is $\sim 10^{-18} \text{ m}^2$ at the base of the seismogenic zone. They concluded that fault weakening by the upflow of mantle fluid at the rate implied by the He flux estimates was plausible.

The mantle CO_2 flux into the fault zone calculated in this study using a spatially restricted He (20 km) and $\text{CO}_2/{}^3\text{He}$ ratio (2×10^9) is $\sim 1\%$ of the flux calculated by Kennedy et al. (1997). This finding suggests that the mantle fluid flux alone is not sufficient to weaken the SAFS at seismogenic depths. Even if the fault zone is assumed to be 100 km wide (more appropriate in the southern SAFS; Wallace, 1990), the flux calculated in this work would be only $\sim 5\%$ of previous estimates. Increasing the length of the SAFS to 3000 km also would have little effect on the flux ($\sim 3\%$ of previous estimates). Therefore, it seems implausible, given the revised fault zone and mantle CO_2 -helium characteristics that the flux of mantle volatiles alone could provide the pressure necessary to weaken the SAFS. However, this study has demonstrated that deep fluids include a mixture of mantle and crustal-derived CO_2 , with a significant contribution of non-mantle (metamorphic) CO_2 ($>95\%$), presumably derived from carbonates and organic carbon-rich sediments (Table 2). This realization is in agreement with investigations of volatiles in rocks and SAFOD drilling mud (Wiersberg and Erzinger, 2011), as well as exhumed faulted rocks, vein fillings, and fluid inclusions (Pili et al., 2011), that the flux of mantle CO_2 is likely subordinate to that associated with metamorphic fluids. We speculate that the mantle and crustal CO_2 fluxes together may be sufficient to regenerate fault-weakening pressures which lead to fault rupture.

Finally, we calculate the mantle CO_2 flux associated with the SAFS using the Kennedy et al. (1997) well data but using the spatially restricted width of degassing (20 km) and mantle $\text{CO}_2/{}^3\text{He}$ ratio

(2×10^9): $1.62 \times 10^{13} \text{ cm}^3 \text{ STP a}^{-1}$ ($7.2 \times 10^8 \text{ mol a}^{-1}$). This value is similar to that derived above for the Big Bend section. Thus, the first-order implication of this observation is that mantle CO_2 fluxes may be uniform along a large section of the SAFS. This observation is somewhat surprising given the difference in geologic slip rates of the different sections of the SAFS ($12\text{--}40 \text{ mm a}^{-1}$ (Working Group on California Earthquake Probabilities (WGCEP), 1995, 2003, 2007; Smith-Konter et al., 2011)). The Carrizo section, including the Big Bend section, has one of the highest slip rates (36 mm a^{-1}) of the SAFS. In this respect, higher flux of mantle volatiles, consequent higher permeability at seismogenic depths, and greater slip rates should be intimately related. Therefore, one might expect higher permeability along the Big Bend section of SAFS and resulting larger flux rates for mantle volatiles, however, this is not the case. In addition, just south of the Carrizo section is the Mojave section of the SAFS, which has a similar slip rate of 33 mm a^{-1} (Smith-Konter et al., 2011), but a flux rate of $3.7 \times 10^7 \text{ mol CO}_2 \text{ a}^{-1}$, which is an order of magnitude lower. The lower flux rate in the Mojave might be explained by the greater distance of the Mojave samples from the SAFS ($\sim 60 \text{ km}$), and the nature of dispersed faults in the Eastern California Shear Zone (Kulongoski et al., 2005). Given the uncertainties associated with various parameters involved in the flux calculations, additional data need to be collected to test for variations in CO_2 fluxes along the strike of the SAFS.

6. Concluding remarks

Helium and CO_2 abundances and isotopic characteristics from 18 groundwater wells near the SAFS were measured in order to determine the origin of fluids and calculate the flux of volatiles in the Big Bend section of the SAFS. The geochemical characteristics indicate a mixture between crustal and mantle-derived volatiles. Helium abundance and isotope values are highest in the wells in the Mil Potrero and Cuddy valleys – closest to the SAFS. However, variability in the helium contents and calculated fluxes over short distances suggests that episodic fracturing and advective fluid flow may influence He distribution in and through the crust. The spatial influence of mantle helium near the fault zone was observed to be $\sim 20 \text{ km}$. The elevated $^3\text{He}/{}^4\text{He}$ ratios are interpreted to be a consequence of a mantle volatile flux through the SAFS. Co-varying He- CO_2 systematics is interpreted to reflect simple mixing between mantle-derived and crustal volatiles. The observed mantle and crustal volatile mixing is best described by a binary mixing curve with a mantle $\text{CO}_2/{}^3\text{He}$ ratio of 2×10^9 .

Based on helium isotope systematics, we calculate a fluid flow rate of 147 mm a^{-1} , up to ~ 37 times higher than previous estimates along the SAFS. However, adopting a restricted width (20 km), the flux of mantle ^3He along the SAFS is estimated to be $7.4 \times 10^3 \text{ cm}^3 \text{ STP a}^{-1}$ ($0.33 \text{ mol } ^3\text{He a}^{-1}$), significantly lower than previous estimates. Adopting the mantle $\text{CO}_2/{}^3\text{He}$ ratio of 2×10^9 , we calculate a CO_2 flux of $1.5 \times 10^{13} \text{ cm}^3 \text{ STP a}^{-1}$ ($6.6 \times 10^8 \text{ mol a}^{-1}$), which is only $\sim 1\%$ of previous estimates. The observed flux of mantle volatiles through the Big Bend section of the SAFS requires that the brittle-ductile transition is permeable. However, this new, lower CO_2 flux estimate suggests that fluxes of mantle volatiles alone are insufficient to produce high pore-fluid pressure and induce fault-weakening (Rice, 1992). The mixing calculated from the helium and carbon components of the groundwater sampled identifies that the flux of CO_2 is dominated by CO_2 derived from fluids from the crust. Therefore, a combination of mantle and metamorphic volatiles may be needed to supply the flux to increase pore-fluid pressure in the seismogenic zone enough to cause fault weakening in the SAFS.

Acknowledgments

The authors thank Bridget Smith-Konter, Ate Visser, and 2 anonymous reviewers for comments, and the California State Water Resources Control Board for support. We especially thank cooperating

well owners and water purveyors for access to wells. Funding was provided by State of California Proposition 50 bonds, administered by the State Water Board, and the National Science Foundation (EAR1014236).

References

- Aeschbach-Hertig, W., 1995. A comment on "Helium sources in passive margin aquifers - New evidence for a significant mantle ^3He source in aquifers with unexpectedly low in situ $^3\text{He}/^4\text{He}$ production". In: Castro, M.C. (Ed.), *Earth Planet. Sci. Lett.* 222 (2004), pp. 897–913. *Earth and Planetary Science Letters* 240 (3–4), 827–829.
- Allard, P., 1992. Global emissions of He-3 by subaerial volcanism. *Geophysical Research Letters* 19 (14), 1479–1481.
- Andrews, J.N., 1985. The isotopic composition of radiogenic helium and its use to study groundwater movement in confined aquifers. *Chemical Geology* 49, 339–351.
- Baker, J.C., Bai, G.P., Hamilton, P.J., Golding, S.D., Keene, J.B., 1995. Continental-scale magmatic carbon dioxide seepage recorded by dawsonite in the Bowen-Gunnedah-Sydney Basin system, eastern Australia. *Journal of Sedimentary Research* A65 (3), 522–530.
- Ballentine, C.J., Burnard, P., 2002. Production of noble gases in the continental crust. In: Porcelli, D., Ballentine, C.J., Wieler, R. (Eds.), *Noble Gases in Geochemistry and Cosmochemistry. : Reviews in Mineralogy and Geochemistry*. Mineralogical Society of America, Washington, pp. 481–538.
- Ballentine, C.J., Burgess, R., Marty, B., 2002. Tracing fluid origin, transport and interaction in the crust. In: Porcelli, D., Ballentine, C.J., Wieler, R. (Eds.), *Noble Gases in Geochemistry and Cosmochemistry. : Reviews in Mineralogy and Geochemistry*. Mineralogical Society of America, Washington, pp. 539–614.
- Barnes, I., Irwin, W.P., White, D.E., 1984. Map Showing World Distribution of Carbon-Dioxide Springs and Major Zones of Seismicity.
- Bethke, C.M., Torgersen, T., Park, J., 2000. The "age" of very old groundwater; insights from reactive transport models. *Journal of Geochimical Exploration* 69–70, 1–4.
- Bredehoeft, J.D., Ingebritsen, S.E., 1990. Degassing of carbon dioxide as a possible source of high pore pressures in the crust. In: Bredehoeft, J.D., Norton, D.L. (Eds.), *The Role of Fluids in Crustal Processes*. National Academy Press, Washington, D.C., pp. 158–164.
- Byerlee, J., 1993. Model for episodic flow of high-pressure water in fault zones before earthquakes. *Geology* 21 (4), 303–306.
- California Division of Mines and Geology, 2000. GIS Data for the Geologic Map of California. CD-ROM 2000-007.
- Cey, B.D., Hudson, G.B., Moran, J.E., Scanlon, B.R., 2008. Impact of artificial recharge on dissolved noble gases in groundwater in California. *Environmental Science and Technology* 42 (4), 1017–1023.
- Chiodini, G., Caliro, S., Cardellini, C., Frondini, F., Inguaggiato, S., Matteucci, F., 2011. Geochemical evidence for and characterization of CO_2 rich gas sources in the epicentral area of the Abruzzo 2009 earthquakes. *Earth and Planetary Science Letters* 304, 389–398.
- Clarke, W.B., Jenkins, W.J., Top, Z., 1976. Determination of tritium by mass spectrometric measurement of He-3. *International Journal of Applied Radiation and Isotopes* 27, 515–522.
- Crossey, L.J., Karlstrom, K.E., Springer, A.E., Newell, D., Hilton, D.R., Fischer, T., 2009. Degassing of mantle-derived CO_2 and He from springs in the southern Colorado Plateau region – Neotectonic connections and implications for groundwater systems. *Bulletin of the Geological Society of America* 121 (7–8), 1034–1053.
- de Leeuw, G.A.M., Hilton, D.R., Gulec, N., Mutlu, H., 2010. Regional and temporal variations in $\text{CO}_2/{}^3\text{He}$, ${}^3\text{He}/{}^4\text{He}$ and d^{13}C along the North Anatolian Fault Zone, Turkey. *Applied Geochemistry* 25 (4), 524–539.
- Deines, P., Langmuir, D., Harmon, R.S., 1974. Stable carbon isotope ratios and the existence of a gas phase in the evolution of carbonate ground waters. *Geochimica et Cosmochimica Acta* 38 (7), 1147–1164.
- DeMets, C.G., Stein, R.G., Seth, S., Argus, D.F., 1987. A revised estimate of the Pacific-North America motion and implications for western North America plate boundary zone tectonics. *Geophysical Research Letters* 14 (9), 911–914.
- Dunai, T.J., Baur, H., 1995. Helium, neon, and argon systematics of the European subcontinental mantle – implications for its geochemical Evolution. *Geochimica et Cosmochimica Acta* 59 (13), 2767–2783.
- Dunai, T.J., Porcelli, D., 2002. Storage and transport of noble gases in the subcontinental lithosphere. In: Porcelli, D., Ballentine, C.J., Wieler, R. (Eds.), *Noble Gases in Geochemistry and Cosmochemistry: Rev. Mineral. Geochem. Mineral. Soc. Am.*, vol. 47 Washington, DC, pp. 371–409.
- Faulkner, D.R., Rutter, E.H., 2001. Can the maintenance of overpressured fluids in large strike-slip fault zones explain their apparent weakness? *Geology* 29 (6), 503–506.
- Fulton, P.M., Saffer, D.M., 2009. Potential role of mantle-derived fluids in weakening the San Andreas Fault. *Journal of Geophysical Research, B: Solid Earth* 114 (7).
- Graham, D.W., 2002. Noble gas isotope geochemistry of mid-ocean ridge and ocean island basalts: characterization of mantle source reservoirs. In: Porcelli, D., Ballentine, C.J., Wieler, R. (Eds.), *Noble Gases in Geochemistry and Cosmochemistry*. Mineralogical Society of America, Washington, pp. 247–318.
- Hill, D.P., Eaton, J.P., Jones, L.M., 1990. Seismicity, 1980–1986. In: Wallace, R.E. (Ed.), *The San Andreas Fault System*. U.S. Geol. Surv. Profess. Pap., California, pp. 115–151.
- Hilton, D.R., Fischer, T.P., Marty, B., 2002. Noble gases and volatile recycling at subduction zones. In: Porcelli, D., Ballentine, C.J., Wieler, R. (Eds.), *Noble Gases in Geochemistry and Cosmochemistry: Rev. Mineral. Geochem. Mineral. Soc. Am.*, vol. 47, pp. 319–370. Washington, DC.
- Hilton, D.R., Ramirez, C.J., Mora-Amador, R., Fischer, T.P., Furi, E., Barry, P.H., Shaw, A.M., 2010. Monitoring of temporal and spatial variations in fumarole helium and carbon dioxide characteristics at Poas and Turrialba Volcanoes, Costa Rica (2001–2009). *Geochemical Journal* 44 (5), 431–440.
- Javoy, M., Pineau, F., Delorme, H., 1986. Carbon and nitrogen isotopes in the mantle. *Chemical Geology* 57 (1–2), 41–62.
- Kennedy, B.M., Kharaka, Y.K., Evans, W.C., Ellwood, A., DePaolo, D.J., Thordsen, J., Ambats, G., Mariner, R.H., 1997. Mantle fluids in the San Andreas fault system, California. *Science* 278 (5341), 1278–1281.
- Kharaka, Y.K., Thordsen, J.J., Evans, W.C., Kennedy, B.M., 1999. Geochemistry and hydromechanical interactions of fluids associated with the San Andreas fault system, California. *Faults and Subsurface Fluid Flow in the Shallow Crust*. Geophys. Monogr. Ser. AGU, Washington, DC, pp. 129–148.
- Kulongoski, J.T., Hilton, D.R., 2002. A quadrupole-based mass spectrometric system for the determination of noble gas abundances in fluids. *Geochemistry, Geophysics, Geosystems* 3, U1–U10.
- Kulongoski, J.T., Hilton, D.R., 2011. Applications of groundwater helium. In: Baskaran, M. (Ed.), *Handbook of Environmental Isotope Geochemistry*. Springer-Verlag, pp. 285–304.
- Kulongoski, J.T., Hilton, D.R., Izbicki, J.A., 2003. Helium isotope studies in the Mojave Desert, California: implications for ground-water chronology and regional seismicity. *Chemical Geology* 202 (1–2), 95–113.
- Kulongoski, J.T., Hilton, D.R., Izbicki, J.A., 2005. Source and movement of helium in the eastern Morongo groundwater Basin: the influence of regional tectonics on crustal and mantle helium fluxes. *Geochimica et Cosmochimica Acta* 69 (15), 3857–3872.
- Kulongoski, J.T., Hilton, D.R., Cresswell, R.G., Hostetler, S., Jacobson, G., 2008. Helium-4 characteristics of groundwaters from Central Australia: comparative chronology with chlorine-36 and carbon-14 dating techniques. *Journal of Hydrology* 348 (1–2), 176–194.
- Lewicki, J.L., Evans, W.C., Hilley, G.E., Sorey, M.L., Rogie, J.D., Brantley, S.L., 2003. Shallow soil CO_2 flow along the San Andreas and Calaveras Faults, California. *Journal of Geophysical Research, B: Solid Earth* 108 (4) (ECV 3-1-3-14).
- Martel, D.J., O'Nions, R.K., Hilton, D.R., Oxburgh, E.R., 1990. The role of element distribution in production and release of radiogenic helium – the Carmmenellis granite, southwest England. *Chemical Geology* 88 (3–4), 207–221.
- Marty, B., Jambon, A., 1987. C^3He in volatile fluxes from the solid Earth: implication for carbon geodynamics. *Earth and Planetary Science Letters* 83, 16–26.
- Marty, B., Jambon, A., Sano, Y., 1989. Helium isotopes and CO_2 in volcanic gases of Japan. *Chemical Geology* 76, 25–40.
- Mathany, T.M., Kulongoski, J.T., Ray, M.C., Belitz, K., 2009. Groundwater quality data in the South Coast Interior Basins study unit, 2008. Results from the California GAMA Program: U.S. Geological Survey Data Series, 463.
- Nur, A., Walder, J., 1990. Time-dependent hydraulics of the Earth's crust. *The Role of Fluids in Crustal Processes*. National Academy Press, pp. 113–127.
- O'Nions, R.K., Oxburgh, E.R., 1988. Helium, volatile fluxes and the development of continental crust. *Earth and Planetary Science Letters* 90, 331–347.
- Pili, E., Poitrasson, F., Gratiat, J.P., 2002. Carbon-oxygen isotope and trace element constraints on how fluids percolate faulted limestones from the San Andreas Fault system; partitioning of fluid sources and pathways. *Chemical Geology* 190 (1–4), 229–248.
- Pili, E., Kennedy, B.M., Conrad, M.E., Gratiat, J.P., 2011. Isotopic evidence for the infiltration of mantle and metamorphic $\text{CO}_2\text{-H}_2\text{O}$ fluids from below in faulted rocks from the San Andreas Fault system. *Chemical Geology* 281 (3–4), 242–252.
- Pineau, F., Javoy, M., 1983. Carbon isotopes and concentrations in mid-oceanic ridge basalts. *Earth and Planetary Science Letters* 62 (2), 239–257.
- Pineau, F., Javoy, M., Bottinga, Y., 1976. $^{13}\text{C}/^{12}\text{C}$ ratios of rocks and inclusions in popping rocks of the Mid-Atlantic Ridge and their bearing on the problem of isotopic composition of deep-seated carbon. *Earth and Planetary Science Letters* 29 (2), 413–421.
- Ray, M.C., Hilton, D.R., Munoz, J., Fischer, T.P., Shaw, A.M., 2009. The effects of volatile recycling, degassing and crustal contamination on the helium and carbon geochemistry of hydrothermal fluids from the Southern Volcanic Zone of Chile. *Chemical Geology* 266 (1–2), 38–49.
- Rice, J.R., 1992. Fault stress, pore pressure distribution, and the weakness of the San Andreas fault. In: Evans, B., Wong, T.F. (Eds.), *Fault Mechanics and Transport Properties of Rocks*. Academic Press, London, pp. 475–503.
- Rogie, J.D., Kerrick, D.M., Chiodini, G., Frondini, F., 2000. Flux measurements of nonvolcanic CO_2 emission from some vents in central Italy. *Journal of Geophysical Research* 105, 8435–8445.
- Sano, Y., Marty, B., 1995. Origin of carbon in fumarolic gas from island arcs. *Chemical Geology* 119, 265–274.
- Schoell, M., 1983. Generic characterization of natural gases. *American Association of Petroleum Geologists Bulletin* 67 (12), 2225–2238.
- Shaw, A.M., Hilton, D.R., Fischer, T.P., Walker, J.A., Alvarado, G.E., 2003. Contrasting He-C relationships in Nicaragua and Costa Rica: insights into C cycling through subduction zones. *Earth and Planetary Science Letters* 214 (3–4), 499–513.
- Sieh, K.E., 1978. Slip along the San Andreas fault associated with the great 1857 earthquake. *Bull. Seismol. Soc. Am.* 68, 1421–1448.
- Sleep, N.H., Blanpied, M.L., 1992. Creep, compaction and the weak rheology of major faults. *Nature* 359 (6397), 687–692.
- Smith-Konter, B.R., Sandwell, D.T., Shearer, P., 2011. Locking depths estimated from geodesy and seismology along the San Andreas Fault System: implications for seismic moment release. *Journal of Geophysical Research, B: Solid Earth* 116 (6).
- Stirling, M.W., Wesnousky, S.G., Shimazaki, K., 1996. Fault trace complexity, cumulative slip, and the shape of the magnitude–frequency distribution for strike-slip faults: a global survey. *Geophysical Journal International* 124, 833–868.
- Torgersen, T., 1980. Controls on pore-fluid concentrations of ${}^4\text{He}$ and ${}^{222}\text{Rn}$ and the calculation of ${}^4\text{He}/{}^{222}\text{Rn}$ ages. *Journal of Geochimical Exploration* 13, 57–75.

- Torgersen, T., O'Donnell, J., 1991. The degassing flux from the solid earth — release by fracturing. *Geophysical Research Letters* 18 (5), 951–954.
- U.S. Geological Survey, 2011. Historic United States earthquakes: USGS Earthquake Hazards Program website. accessed April 6, 2011, at http://earthquake.usgs.gov/earthquakes/states/historical_state.php.
- Wallace, R.E., 1990. The San Andreas fault system, California. US Geological Survey Professional Paper, 1515.
- Weiss, R.F., 1968. Piggyback sampler for dissolved gas studies on sealed water samples. *Deep Sea Research* 15, 721–735.
- Weiss, R.F., 1971. Solubility of helium and neon in water and seawater. *Journal of Chemical and Engineering Data* 16, 235–241.
- Whiticar, M.J., 1994. Correlation of natural gases with their sources. *The Petroleum System — From Source to Trap*, pp. 261–283.
- Wiersberg, T., Erzinger, J., 2008. Origin and spatial distribution of gas at seismogenic depths of the San Andreas Fault from drill-mud gas analysis. *Applied Geochemistry* 23 (6), 1675–1690.
- Wiersberg, T., Erzinger, J., 2011. Chemical and isotope compositions of drilling mud gas from the San Andreas Fault Observatory at Depth (SAFOD) boreholes: implications on gas migration and the permeability structure of the San Andreas Fault. *Chemical Geology* 284 (1–2), 148–159.
- Working Group on California Earthquake Probabilities (WGCEP), 1995. Seismic hazards in southern California: probable earthquakes, 1994–2024. *Bulletin of the Seismological Society of America* 85, 379–439.
- Working Group on California Earthquake Probabilities (WGCEP), 2003. Earthquake probabilities in the San Francisco bay region: 2002–2031. U.S. Geol. Surv. Open-File Rept. 2003-214.
- Working Group on California Earthquake Probabilities (WGCEP), 2007. The Uniform California Earthquake rupture forecast, version 2 (UCERF 2). U.S. Geol. Surv. Open-File Rept. 2007-1437.
- Wycherley, H., Fleet, A., Shaw, H., 1999. Some observations on the origins of large volumes of carbon dioxide accumulations in sedimentary basins. *Marine and Petroleum Geology* 16 (6), 489–494.